Biochemical and Biophysical Research Communications 434 (2013) 48–53

Contents lists available at SciVerse ScienceDirect

Biochemical and Biophysical Research Communications

journal homepage: www.elsevier.com/locate/ybbrc

Structural insights into the coordination of iron by *Thermus thermophilus* HB8 ferric binding protein A

Qing Wang [a,b], Qingyu Lu [b], Qiyun Zhou [c], Xinquan Wang [b], Xiaoqing Liu [a,*]

[a] College of Life Sciences, Capital Normal University, Beijing 100048, People's Republic of China
[b] Center for Structural Biology, School of Life Sciences, Ministry of Education Key Laboratory of Protein Science, Tsinghua University, Beijing 100084, People's Republic of China
[c] Key Laboratory of Bioactive Substances and Functional Foods, College of Applied Sciences and Humanities, Beijing Union University, Beijing 100191, People's Republic of China

ARTICLE INFO

Article history:
Received 11 March 2013
Available online 29 March 2013

Keywords:
Ferric binding protein A
Thermus thermophilus HB8
Conformation change

ABSTRACT

The ferric binding protein belongs to the substrate-binding protein super-family and transports ferric ions across the periplasmic space in gram negative bacteria. This process involves the binding and release of ferric ions through conformational changes of the ferric binding protein, and the assistance of a synergistic anion. Here we report the crystal structure of *Thermus thermophilus* HB8's (TtFbpA) ferric binding protein A in four different forms, which represent the apo state (apo-TtFbpA), the carbonate-bound state ($TtFbpACO_3$),and the iron- and carbonate-bound state ($TtFbpAFeCO_3$). The ferric ion in $TtFbpAFeCO_3$ is bound by three tyrosine residues from TtFbpA and one synergistic carbonate ion. Structural comparisons among the three different states reveal the molecular mechanisms of iron-binding by TtFbpA. Our results, together with previous studies on other bacterial periplasmic ferric binding proteins, provide a complete understanding of the structural basis for iron binding and release in the periplasm of gram-negative bacteria.

1. Introduction

The acquisition of elemental iron is vital for the growth and survival of most bacteria, including those which infect vertebrates [1]. Therefore, vertebrate hosts may limit iron availability as a mechanism to protect against bacterial infections [2]. For example, in humans, the iron-binding proteins transferrin (Tf) and lactoferrin (Lf) bind extracellular free iron with extremely high affinity, which results in very low concentrations of free iron. This binding of free iron helps to limit the growth of many infectious microorganisms. On the other side of the host–pathogen interaction, bacteria have developed high-affinity iron-uptake systems to obtain iron from host iron-binding proteins or the environment [3].

There are two different iron-acquisition mechanisms in bacteria. When using the first mechanism, bacteria synthesize low-molecular weight organic chelators to compete for Tf- and Lf-bound iron and then transport iron in a chelated form [4]. The second mechanism is chelator-independent and is initiated by bacteria surface-associated membrane proteins specific to Tf and Lf [5]. In pathogens such as Pasteurellaceae and Neisseriaceae, the bacterial outer membrane receptor is composed of two proteins: Tf binding protein A (TbpA) and lipoprotein TbpB. Upon binding of Tf and Lf by TbpA/TbpB, the bound ferric ion is released and transported across the outer membrane into the periplasmic space [5]. In the periplasmic space, the free ferric ion is then bound by ferric binding protein A (FbpA) to form a temporary complex which transports iron across the periplasm, to the inner membrane [6]. The subsequent transport of ferric ions across the inner membrane after release from FbpA is facilitated by the ATP binding cassette (ABC) free iron transporter which consists of the inner membrane permease FbpB and the cytoplasmic ATPase FbpC [7]. Key to this process is the reversible binding of ferric ion by FbpA, which facilitates the movement of iron in the periplasm.

In metazoans, transferrins are composed of two globular lobes that can be further subdivided into two sub-domains, each of which can bind a ferric ion [8]. The ferric ion is coordinated by two tyrosines, a histidine, an aspartic acid and a carbonate anion [9]. Ferric binding protein A in bacteria has been called the "bacterial transferrin" due to its overall structure similarity to a single lobe of metazoan transferrin [10]. The structure of FbpA from a number of bacterial strains have been determined [10–17], and these bacterial FbpAs display a very similar overall topology. Bacterial FbpAs are composed of an N- and a C-domain, which are connected by two short strands that act as a hinge. The ligand-binding site is buried between the N- and C-domains. However, these structures also reveal some variability in the mechanisms by which iron is coordinated with FbpA. The first coordination form, found in the Yersinia enterocolitica FbpA (YfuA), utilizes five amino acids including two tyrosines, a histidine, a glutamine, and an aspartic acid and a water molecular to form hexa-coordination [16]. The second geometry for the coordination of a ferric ion, found in the

* Corresponding author.
E-mail address: liuxq@mail.cnu.edu.cn (X. Liu).

0006-291X/$ - see front matter © 2013 Elsevier Inc. All rights reserved.
http://dx.doi.org/10.1016/j.bbrc.2013.03.068

Haemophilus influenzae FbpA, possesses a set of four amino acids, similar to YfuA, but in *H. influenza* the aspartic acid is replaced by a phosphate anion in the coordination complex [11]. A novel class of iron-binding proteins were reported in the *cyanobacteria Synechocystis* 6803, and in this organism the ferric ion is bound via four tyrosines and one histidine [18]. The fourth iron-binding coordination, represented by *Mannheimia haemolytica* ferric binding protein A (MhFbpA), differs from the other characterized human and bacterial ferric ion transport proteins [15,17]. It utilizes only three tyrosine residues and a synergistic carbonate to coordinate a ferric ion in an asymmetric manner.

In this study, we present high resolution crystal structures of the *Thermus thermophilus* HB8 ferric binding protein (TtFbpA) in three different states: the apo-TtFbpA form (a fully opened conformation without any bound ligand); the TtFbpACO_3 form (a carbonate-bound open conformation with a solvent exposed iron-binding site); and the TtFbpAFeCO_3 form (a fully closed conformation with bound ferric ion and a carbonate ion). These three structures provide the precise atomic details of ferric ion coordination, which have allowed us to elucidate the molecular mechanism of iron-binding and release by TtFbpA.

2. Materials and methods

2.1. Protein purification, crystallization, and diffraction data collection

The methods used for protein purification, crystallization, and diffraction data collection have been reported previously [19]. In brief, we grew four different crystal forms of TtFbpA using the vapor diffusion hanging drop method. Full-length TtFbpA (residues 1–330) with a C-terminal His tag was expressed and purified from *Escherichia coli*. An HBS buffer (10 mM HEPES pH 7.2, 150 mM NaCl). with an additional 10 mM sodium bicarbonate was used to purify ferric-bound TtFbpA expressed in *E. coli*. The final concentrated protein sample was orange in color and the presence of ferric ion was confirmed by atomic absorption spectrophotometry [19]. Colorless form I crystals were obtained at room temperature against 0.2 M ammonium acetate, 0.1 M sodium acetate trihydrate pH 4.6, and 30% (w/v) PEG 4000 with TtFbpA sample expressed in *E. coli* and purified with HBS buffer. Even with the ferric-bound orange TtFbpA protein sample, colorless crystals were still obtained at room temperature from drops equilibrated against a reservoir consisting of 0.2 M Li_2SO_4, 0.1 M Bis-Tris pH 6.5, and 28% (w/v) PEG 3350 (form II) or 0.2 M NaCl, 0.1 M Bis-Tris pH 5.5, and 25% (w/v) PEG 3350 (form III). Orange form IV crystals grew at room temperature in 0.2 M $MgCl_2$, 0.1 M HEPES pH 7.5, and 26% (w/v) PEG 3350. Prior to data collection, all crystals were transferred to a cryo-solution containing 20% glycerol with mother liquor and then flash-cooled. Data collection was performed at 100 K using a wavelength of 0.9791 Å at the BL17U beamline of the Shanghai synchrotron-radiation source (SSRF) with a MAR 225 CCD detector system. Initial molecular-replacement trials with available FbpA structures as search models failed to provide any clear solutions. Therefore, a Br-derivative dataset of the form I crystal was collected with the peak wavelength of 0.9196 Å. All data were processed and scaled with the HKL2000 software package [20]. Data collection and processing statistics are listed in the previous preliminary crystallography report [19].

2.2. Structure determination and refinement

The form I TtFbpA structure was solved using a single-wavelength anomalous dispersion (SAD) method. The positions of Br were determined using the program SHELXD [21] and initial phases were calculated with the program SHELXE [22] as part of the HKL2MAP package [23]. Density modification was conducted using DM in the CCP4 suite [24]. The resulting electron density map was of excellent quality, allowing an automatic chain trace to be performed with the program Arp/wARP [25]. The form II and form III TtFbpA structures were determined with the molecular replacement method using the form I TtFbpA crystal structure as a search model. For form IV crystal structure determination, the N- and C-terminal domains had to be searched independently to solve the structure. All molecular replacement searches were conducted with the program PHASER in the CCP4 suite [26]. Iterative cycles of manual model building with the program COOT and structure refinement with the program PHENIX were conducted to complete and correct the models [27]. During the late stage of model building and refinement, the carbonate ion, ferric ion, and water molecules were added based on the $2|F_o| - |F_c|$ and $|F_o| - |F_c|$ maps.

3. Results

3.1. Model completeness and quality

Form I crystals were found to belong to the orthorhombic space group $P2_12_12_1$ (a = 42.1, b = 139.3, c = 326.3 Å) with six TtFbpA molecules in the asymmetric unit. The structure was determined at 1.91 Å resolution with final R values of R_{cryst} = 16.3% and R_{free} = 20.7%. The final six TtFbpA models all included residues Thr23-Leu330, with 22 N-terminal residues absent due to lack of interpretable electron density. Form II crystals were found to belong to the orthorhombic space group $P2_12_12_1$ (a = 42.3, b = 139.2, c = 218.9 Å) with four TtFbpA molecules (residues Thr23-Leu330), each bound with a carbonate, in the asymmetric

Table 1
Refinement statistics.

	TtFbpA (form I)	TtFbpACO_3 (form II)	TtFbpACO_3 (form III)	TtFbpAFeCO_3 (form IV)
Resolution (Å)	36.0–1.91	40.5–2.07	36.3–1.89	42.5 – 2.50
Completeness for range (%)	94.8	91.6	95.4	99.1
Reflections	141958	73688	42398	22428
R_{work}/R_{free}	0.163/0.207	0.199/0.260	0.172/0.225	0.169/0.218
Number of protein atoms	14336	9552	4802	4802
Number of water atoms	1633	382	409	242
Ions	0 Fe/0 carbonate	0 Fe/4 Carbonate	0 Fe/2 Carbonate	2 Fe/2 Carbonate
Mean B-factors (Å^2)				
Protein atoms	27.1	33.2	46.6	25.2
Water atoms	35.6	33.6	32.6	28.4
Ions		42.7	35.6	19.4
Root mean square deviations				
Bond lengths (Å)	0.007	0.007	0.006	0.008
Bond angles (°)	1.031	1.042	1.041	1.050

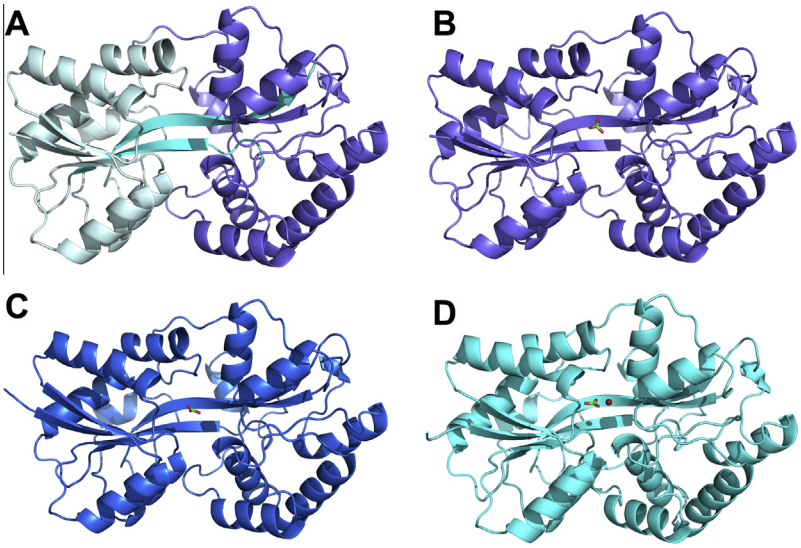

Fig. 1. Ribbon diagrams of TtFbpA in four different crystal forms. (A) In the form I structure, the N-domain, C-domain and connecting β strands are colored with light blue, dark blue, and cyan, respectively. (B) The form II structure with bound carbonate. (C) The form III structure with bound carbonate. (D) The form IV structure with a bound ferric ion and carbonate. (For interpretation of the references to color in this figure legend, the reader is referred to the web version of this article.)

unit. The structure was determined at 2.07 Å resolution with final *R* values of R_{cryst} = 19.9% and R_{free} = 26.0%. Form III crystals were found to belong to the monoclinic space group $P2_1$ (a = 66.5, b = 61.7, c = 73.9 Å, β = 111.7°) with two TtFbpA molecules (residues Ser21-Leu330), each also bound with a carbonate, in the asymmetric unit. The final *R* values are R_{cryst} = 17.2% and R_{free} = 22.5% and the structure was determined at a resolution of 1.89 Å. The orange form IV crystals were found to belong to the trigonal space group $P3_121$ (a = 63.6, b = 63.6, c = 266.7 Å, $\alpha = \beta = 90.0$, $\gamma = 120°$) with two TtFbpA molecules (residues Ser21-Leu330), each bound with a carbonate and a ferric ion, in the asymmetric unit. The structure was determined at a resolution of 2.50 Å with final R values of R_{cryst} = 16.9% and R_{free} = 21.8%. Ramachandran plots computed with PROCHECK show that 95.2%, 93.7%, 94.9%, and 93.4% of the modeled residues are in the most favorable region for form I–IV structures respectively, and that no residues were found in disallowed regions [28]. The structural refinement statistics are listed in Table 1.

3.2. Overall structure

Bacterial periplasmic ligand-binding proteins have a similar structure, which consists of two globular domains connected by a pair of antiparallel β strands, but have low sequence homology [29]. The ligand-binding site is at the cleft between the two domains, and the interlinking β strands act as flexible hinges to allow

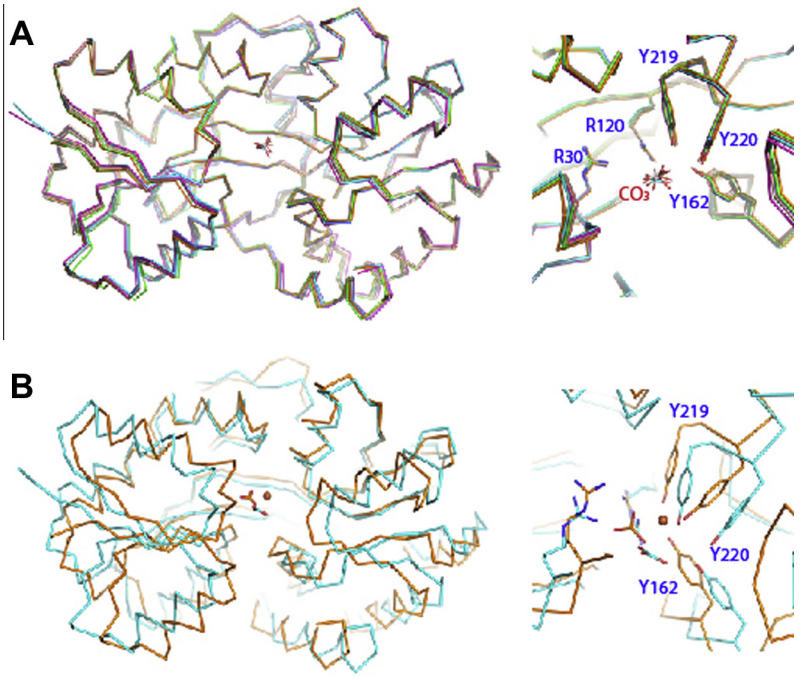

Fig. 2. Comparison of TtFbpA in different forms. (A) A total of six independent $TtFbpACO_3$ monomers with bound carbonate from our form II and III structures are aligned with the apo-TtFbpA monomer (our form I, cyan). (B) The $TtFbpAFeCO_3$ monomer (our form IV, orange) is aligned with the apo-TtFbpA monomer (our form I, cyan). (For interpretation of the references to color in this figure legend, the reader is referred to the web version of this article.)

the rotation of the two globular domains with respect to one another. This large-scale inter-domain conformational change helps to establish the opened and closed state of the protein, which is necessary to perform its ligand acquisition and release functions [29]. TtFbpA belongs to the ligand-binding protein superfamily and its N- and C-terminal domains are both composed of twisted mixed β-sheets surrounded by α-helices (Fig. 1A). The N-terminal domain (residues Thr23-Trp114 and Leu253-Val291) consists of six helices and three α strands, while the C-terminal domain (residues Pro128Ala241 and Ala292-Ala330) is composed of six helices and two β strands (Fig. 1A). The two domain-swapping anti-parallel β strands in TtFbpA are composed of residues Val115Asn127 and residues Gly242-Leu252 (Fig. 1A).

We studied four different crystal forms of the TtFbpA. Our form I TtFbpA structure is in a fully open state and inspection of the electron density map did not reveal obvious density for a ferric ion or a synergistic anion at the binding site. Our Form II and form III structures are also in an open state, and are very similar to our form I structure (Fig. 1B and C). For example, the r.m.s.d. for all aligned Cα atoms is 0.43 Å between form II and form I structures and 0.63 Å between form III and form I structures. Although these forms have adopted a similar open state, a carbonate can be placed close to the ferric ion binding site in the form II and form III structures based on the $2|F_o| - |F_c|$ and $|F_o| - |F_c|$ electron density maps (Fig. 1B and C). Our form IV structure represents a fully closed state bound to a ferric ion and a synergistic carbonate ion (Fig. 1D). For the following description and discussion, we use apo-TtFbpA to refer to the form I structure, $TtFbpACO_3$ to refer to the form II and form III structures with bound carbonate, and $TtFbpAFeCO_3$ to refer to the form IV structure with bound ferric ion and carbonate.

3.3. Ligand-binding site

$TtFbpACO_3$ adopts a fully open state with a bound carbonate. Although the orientation of the carbonate ion varies in the six independent $TtFbpACO_3$ models from our form II and III structures, its general location in $TtFbpACO_3$ is conserved (Fig. 2A). The exact location of the carbonate is determined by its specific interactions with surrounding residues (Fig. 2A). The TtFbpA residues Arg30 and Arg120 provide a small area of positive charge to attract the carbonate, which then interacts with TtFbpA's Tyr162, Tyr219, and Tyr220 residues (Fig. 3A). Most importantly, the side chain conformations of these interacting residues are conserved in both TtFbpA and $TtFbpACO_3$ structures (Fig. 2A). Therefore, despite the fact that the overall large-scale inter-domain conformation and the local binding site conformation do not change significantly, we suggest that the binding of the carbonate prepares the protein for the subsequent loading of a ferric ion.

In the $TtFbpAFeCO_3$ structure, the N- and C-terminal domains rotate toward each other around the two β-strands that run along the back of the protein and clamp down towards the ferric binding site, forming a fully closed state (Fig. 2B). After the binding of the ferric ion, TtFbpA residues Tyr162, Tyr219 and Tyr210, and the synergistic carbonate ion, are more compact (Fig. 2B). The distances between the OH atoms in these three tyrosine residues are 3.2, 3.0 and 2.7 Å, respectively, in the $TtFbpAFeCO_3$ structure. This is slightly reduced from the distances of 3.5, 2.9 and 3.1 Å in the $TtFbpACO_3$ structure.

3.4. Ferric ion coordination

The ferric ion in the $TtFbpAFeCO_3$ structure is chelated by three tyrosine residues (Tyr162, Tyr219 and Tyr220) from the C-terminal domain and two additional interactions with the associated carbonate (Fig. 3B). The distances from the ferric ion to the three OH atoms of Tyr162, Tyr219 and Tyr220 are 1.8, 1.9 and 1.9 Å,

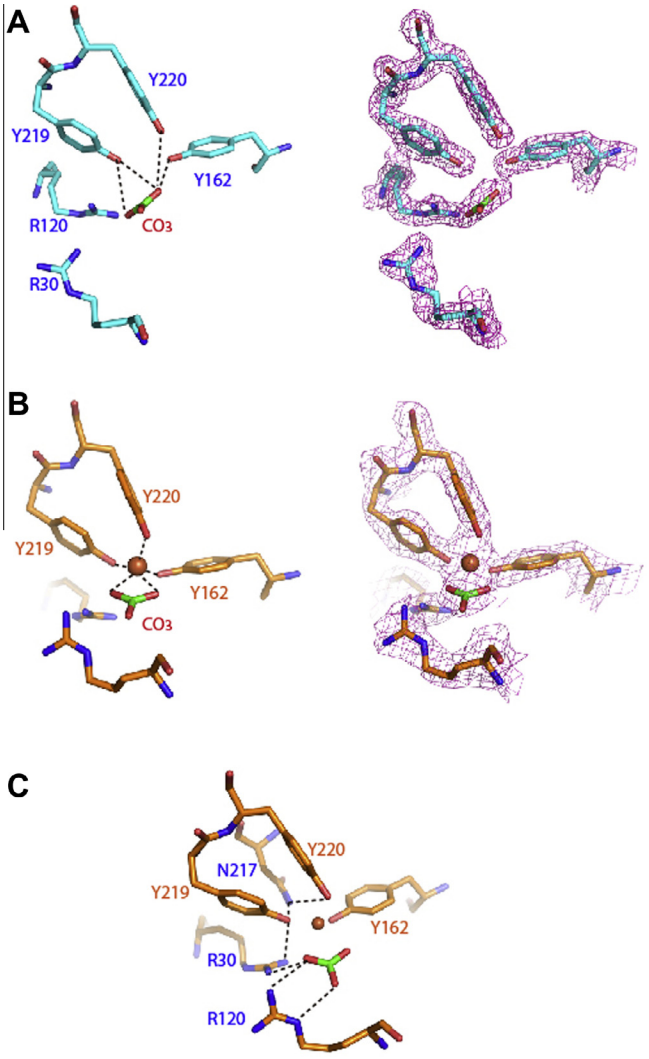

Fig. 3. The TtFbpA ligand-binding site. (A) The carbonate in the ligand-binding site of $TtFbpACO_3$. (B) The carbonate and ferric ions in the ligand-binding site of $TtFbpAFeCO_3$. (C) Interactions between the ferric-coordinating carbonate and tyrosine residues with outside residues.

respectively. The distances from the ferric ion to the carbonate's two oxygen atoms are slightly longer, at lengths of 2.2 and 2.3 Å. Besides the interactions with the bound ferric ion, these tyrosine residues and the carbonate ion also interact with the outside second shell of TtFbpA residues that help to firmly hold their respective positions to coordinate with the ferric ion. Both Arg30 and Arg120 have hydrogen-bonding interactions with the carbonate (Fig. 3C). Arg120 forms hydrogen bonds with Tyr219, and Asn217 forms hydrogen bonds with Tyr162 and Tyr219 (Fig. 3C). These interactions improve the iron-tyrosine interactions by increasing the electro-negativity of the tyrosine hydroxyls. The utilization of three tyrosine residues and a carbonate to coordinate ferric ion has been previously reported in the structure of *M. haemolytica* ferric binding protein A (MhFbpA) [15]. Structural alignment based on the two consecutive tyrosine residues (Tyr219 and Tyr 220 in TtFbpA and Tyr197 and Tyr198 in MhFbpA) shows that the coordination of binding site residues and carbonate to the ferric ion is very similar in TtFbpA and MhFpbA (Fig. 3D). The major difference between these two orthologous proteins is the position of the third tyrosine residue (Tyr162 in TtFbpA and Tyr142 in MhFbpA) (Fig. 3D).

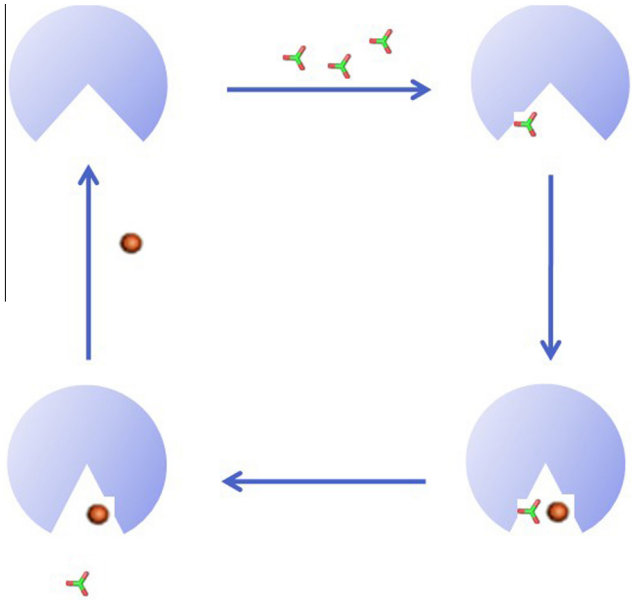

Fig. 4. Model of how bacterial ferric iron binding protein A binds and releases iron and carbonate in the periplasm.

4. Discussion

In this study, we present high resolution crystal structures of TtFbpA in three different states: apo-TfFbpA, TtFbpACO_3, and TtFbpAFeCO_3. apo-TtFbpA represents the open conformation without a bound ferric ion or synergistic anion. TtFbpACO_3 also represents the open conformation, but with a bound carbonate anion. TtFbpAFeCO_3 represents a fully closed conformation with a bound ferric ion and a bound carbonate anion. MhFbpA has also been structurally analyzed in three different states: MhFbpAFe, MhFbpAFeCO_3, and apo-MhFbpA [13]. The TtFbpAFeCO_3 and MhFbpAFeCO_3 structures are very similar as both adopt a fully closed conformation. However, the apo-MhFbpA is iron-free, but adopts a closed conformation with a bound formate anion, which differs from the carbonate-bound open conformation of TtFbpACO_3 which we studied. Similarly, MhFbpAFe adopts a unique iron-bound open conformation, which differs from the open conformation of TtFbpA that we studied. It has been proposed that the three MhFbpA states represent snapshots during the progress of iron release [13], and that the removal of the carbonate, either facilitated by protonation through a reduction in pH in the microenvironment or displacement by other synergistic anions, results in the opening of MhFbpA and a lowering of the affinity for ferric ions. It has been further suggested that the carbonate promotes a closed conformation of MhFbpA by stitching the N- and C-terminal domains together through hydrogen bonding interactions [13]. This conclusion is based on the observation that the removal of a carbonate from MhFbpAFeCO_3 results in an open conformation with a bound ferric ion (apo-MhFbpA). We propose that the three different states of TtFbpA that we present represent snapshots during the progress of iron acquisition. For apo-TtFbpA, in an open state without a bound synergistic anion, binding affinity for ferric ions is low. Unlike in MhFbpA, we did not find that the binding of a carbonate (TtFbpACO_3) induces the switch from an open to a closed conformation in TtFbpA, as the TtFbpACO_3 still has an open conformation. However, we suggest that the ligand-binding microenvironment in TtFbpACO_3 prepares the protein for the recruitment of a ferric ion, and that the binding of these two ions are further strengthened by the clamping together of the N- and C-terminal domains.

Our results, in combination with previous studies on MhFbpA, present a complete view of iron binding and release by the anion-dependent FbpA by providing structural snapshots at a number of different states (Fig. 4). The FbpA in the apo state (S1) has an open conformation and first binds to a synergistic anion (S2). The FbpA bound to carbonate remains in an open state. Next, a ferric ion is recruited (S3) and FbpA switches to a closed conformation and becomes a stable FbpA-iron-anion complex. This stable complex transfers across the periplasm and the release of ferric ion starts when the synergistic anion leaves FbpA (S4), at this point FbpA switches back to the open conformation (S5). The last step is the release of the ferric ion, and at this point the FbpA is in its apo, open, state (S1) again, and is ready for the next cycle of iron transportation.

Acknowledgments

The diffraction data was collected at Shanghai Synchrotron Research Facility (SSRF) Beamline BL17U, and we thank J. H. He, S. Huang, and L. Tang for on-site assistance at SSRF.This work was supported by the National Natural Science Foundation of China (31070067), the Ministry of Education (20100002110001 and 20090002120036) and Scientific Research Common Program of Beijing Municipal Commission of Education (KM200911417001).

References

[1] V. Braun, H. Killmann, Bacterial solutions to the iron-supply problem, Trends Biochem. Sci. 24 (1999) 104–109.
[2] E.D. Weinberg, Iron withholding: a defense against infection and neoplasia, Physiol. Rev. 64 (1984) 65–102.
[3] C. Wandersman, P. Delepelaire, Bacterial iron sources: from siderophores to hemophores, Annu. Rev. Microbiol. 58 (2004) 611–647.
[4] J.B. Neilands, Siderophores: structure and function of microbial iron transport compounds, J. Biol. Chem. 270 (1995) 26723–26726.
[5] S.D. Gray-Owen, A.B. Schryvers, Bacterial transferrin and lactoferrin receptors, Trends Microbiol. 4 (1996) 185–191.
[6] C.J. Parker Siburt, T.A. Mietzner, A.L. Crumbliss, FbpA – A bacterial transferrin with more to offer, Biochim. Biophys. Acta 2012 (1820) 379–392.
[7] W. Koster, ABC transporter-mediated uptake of iron, siderophores, heme and vitamin B12, Res. Microbiol. 152 (2001) 291–301.
[8] E.N. Baker, B.F. Anderson, H.M. Baker, R.T. MacGillivray, S.A. Moore, N.A. Peterson, S.C. Shewry, J.W. Tweedie, Three-dimensional structure of lactoferrin. Implications for function, including comparisons with transferrin, Adv. Exp. Med. Biol. 443 (1998) 1–14.
[9] B.F. Anderson, H.M. Baker, G.E. Norris, D.W. Rice, E.N. Baker, Structure of human lactoferrin: crystallographic structure analysis and refinement at 2.8 A resolution, J. Mol. Biol. 209 (1989) 711–734.
[10] M. Guo, I. Harvey, W. Yang, L. Coghill, D.J. Campopiano, J.A. Parkinson, R.T. MacGillivray, W.R. Harris, P.J. Sadler, Synergistic anion and metal binding to the ferric ion-binding protein from *Neisseria gonorrhoeae*, J. Biol. Chem. 278 (2003) 2490–2502.
[11] C.M. Bruns, D.S. Anderson, K.G. Vaughan, P.A. Williams, A.J. Nowalk, D.E. McRee, T.A. Mietzner, Crystallographic and biochemical analyses of the metal-free *Haemophilus influenzae* Fe3+-binding protein, Biochemistry 40 (2001) 15631–15637.
[12] S.A. Tom-Yew, D.T. Cui, E.G. Bekker, M.E. Murphy, Anion-independent iron coordination by the Campylobacter jejuni ferric binding protein, J. Biol. Chem. 280 (2005) 9283–9290.
[13] A. Badarau, S.J. Firbank, K.J. Waldron, S. Yanagisawa, N.J. Robinson, M.J. Banfield, C. Dennison, FutA2 is a ferric binding protein from Synechocystis PCC 6803, J. Biol. Chem. 283 (2008) 12520–12527.
[14] S.R. Shouldice, D.R. Dougan, R.J. Skene, L.W. Tari, D.E. McRee, R.H. Yu, A.B. Schryvers, High resolution structure of an alternate form of the ferric ion binding protein from *Haemophilus influenzae*, J. Biol. Chem. 278 (2003) 11513–11519.
[15] S.R. Shouldice, R.J. Skene, D.R. Dougan, G. Snell, D.E. McRee, A.B. Schryvers, L.W. Tari, Structural basis for iron binding and release by a novel class of periplasmic iron-binding proteins found in gram-negative pathogens, J. Bacteriol. 186 (2004) 3903–3910.
[16] S.R. Shouldice, D.E. McRee, D.R. Dougan, L.W. Tari, A.B. Schryvers, Novel anion-independent iron coordination by members of a third class of bacterial periplasmic ferric ion-binding proteins, J. Biol. Chem. 280 (2005) 5820–5827.
[17] S.R. Shouldice, D.R. Dougan, P.A. Williams, R.J. Skene, G. Snell, D. Scheibe, S. Kirby, D.J. Hosfield, D.E. McRee, A.B. Schryvers, L.W. Tari, Crystal structure of *Pasteurella haemolytica* ferric ion-binding protein A reveals a novel class of bacterial iron-binding proteins, J. Biol. Chem. 278 (2003) 41093–41098.

[18] N. Koropatkin, A.M. Randich, M. Bhattacharyya-Pakrasi, H.B. Pakrasi, T.J. Smith, The structure of the iron-binding protein, FutA1, from Synechocystis 6803, J. Biol. Chem. 282 (2007) 27468–27477.

[19] Q. Wang, L. Chang, X. Wang, X. Liu, Expression, crystallization and preliminary X-ray analysis of a ferric binding protein from *Thermus thermophilus* HB8, Acta Crystallogr. Sect. F Struct. Biol. Cryst. Commun. 67 (2011) 723–726.

[20] Z. Otwinowski, W. Minor, Processing of X-ray diffraction data collected in oscillation mode, Macromol. Crystallogr., Pt A 276 (1997) 307–326.

[21] T.R. Schneider, G.M. Sheldrick, Substructure solution with SHELXD, Acta Crystallogr. D Biol. Crystallogr. 58 (2002) 1772–1779.

[22] S. Gm, Macromolecular phasing with SHELXE, Z. Kristallogr. 217 (2002) 644–650.

[23] T. Pape, T.R. Schneider, HKL2MAP: a graphical user interface for macromolecular phasing with SHELX programs, J. Appl. Cryst. 37 (2004) 843–844.

[24] Collaborative Computational Project, N. 4, The CCP4 suite: programs for protein crystallography, Acta Crystallogr. D Biol. Crystallogr. 50 (1994) 760–763.

[25] A. Perrakis, M. Harkiolaki, K.S. Wilson, V.S. Lamzin, ARP/wARP and molecular replacement, Acta Crystallogr. D Biol. Crystallogr. 57 (2001) 1445–1450.

[26] A.J. McCoy, R.W. Grosse-Kunstleve, P.D. Adams, M.D. Winn, L.C. Storoni, R.J. Read, Phaser crystallographic software, J. Appl. Crystallogr. 40 (2007) 658–674.

[27] P.D. Adams, R.W. Grosse-Kunstleve, L.W. Hung, T.R. Ioerger, A.J. McCoy, N.W. Moriarty, R.J. Read, J.C. Sacchettini, N.K. Sauter, T.C. Terwilliger, PHENIX: building new software for automated crystallographic structure determination, Acta Crystallogr. D Biol. Crystallogr. 58 (2002) 1948–1954.

[28] R.A. Laskowski, M.W. MacArthur, D.S. Moss, J.M. Thornton, PROCHECK: a program to check the stereochemical quality of protein structures, J. Appl. Cryst. 26 (1993) 283–291.

[29] R.P. Berntsson, S.H. Smits, L. Schmitt, D.J. Slotboom, B. Poolman, A structural classification of substrate-binding proteins, FEBS Lett. 584 (2010) 2606–2617.